HYPERSONIC FLIGHT STRATEGIES FOR SUPERSONIC RETROPROPULSION AT MARS

BY

CHRISTOPHER G. LORENZ

THESIS

Submitted in partial fulfillment of the requirements
for the degree of Master of Science in Aerospace Engineering
in the Graduate College of the
University of Illinois at Urbana-Champaign, 2017

Urbana, Illinois

Adviser:

Assistant Professor Zachary R. Putnam

ABSTRACT

Future large-scale Mars surface exploration missions require landed masses beyond the capability of current entry, descent, and landing technology. High-mass missions will likely use supersonic retropropulsion to increase landed mass, a paradigm shift from current supersonic parachute systems. This work explores hypersonic flight strategies appropriate for use with supersonic retropropulsion systems at Mars. Optimal control techniques are used to determine hypersonic bank-angle profiles that achieve favorable supersonic retroprolusion ignition states. Bang-bang control in the hypersonic flight regime is shown to be optimal for targeting specific state values at terminal descent initation and for minimizing propellant use during propulsive descent. A trade-off between altitude and flight-path angle at supersonic retropropulsion ignition is identified. Minimum-propellant propulsive descent trajectories are identifed and studied parametrically. Results show that hypersonic ballistic coefficient and lift-to-drag ratio have the largest effects on minimum propellant mass fraction; changes to the vehicle state at entry interface have a smaller effect. The space of reachable supersonic retropropulsion ignition states is presented over a range of vehicle and trajectory parameters of interest. Results indicate execution of an appropriate hypersonic flight strategy can significantly reduce the amount of propellant required for supersonic retropulsion systems performing powered descent and landing at Mars.

TABLE OF CONTENTS

NOMENCLATURE

C_D = hypersonic drag coefficient

g_0 = acceleration due to gravity at surface of Earth, m/s^2

g_m = acceleration due to gravity at surface of Mars, m/s^2

h = altitude, m

h_{ref} = reference density altitude, m

H_{scale} = atmospheric scale height, m

H = Hamiltonian

I_{sp} = specific impulse, s

J = cost function

L/D = hypersonic lift-to-drag ratio

m = mass, kg

p = costate

R_m = mean radius of Mars, m

S = switching function

A_{ref} = aerodynamic reference area, m^2

T = thrust magnitude, N

t = time, s

u = optimal control

V = atmosphere-relative velocity magnitude, m/s

β = $m/(C_D A_{ref})$, ballistic coefficient, kg/m^2

γ = flight-path angle, positive above local horizontal, rad

ρ = atmospheric density, kg/m^3

ρ_{ref} = reference atmospheric density, kg/m^3

σ = bank angle, rad

CHAPTER 1: INTRODUCTION

Current supersonic parachute decelerator technologies for Mars entry, descent, and landing (EDL) scale poorly with increasing vehicle mass. Supersonic retropropulsion (SRP) technology has been shown to scale well with increasing landed mass.[1] As a result, future large-mass Mars surface missions will likely use supersonic retropropulsion to perform terminal descent and landing.[2]

Entry vehicle diameters are limited by launch vehicle payload fairing maximum-diameter constraints. In the absence of a deployable drag area, larger payload masses increase entry vehicle ballistic coefficient. EDL systems capable of landing vehicles with larger ballistic coefficients enable larger payload masses to be delivered to the surface of Mars. Figure 1 shows the feasible regions in which parachute deployment is possible for current-state-of-the-art disk-gap-band parachutes. Vehicles with ballistic coefficients in excess of 150 kg/m^2 do not pass through this parachute deployment envelope, assuming a hypersonic lift-to-drag ratio of 0.18. Either further advances in parachute technology or an alternate terminal descent method is necessary to land larger ballistic coefficient vehicles on Mars.

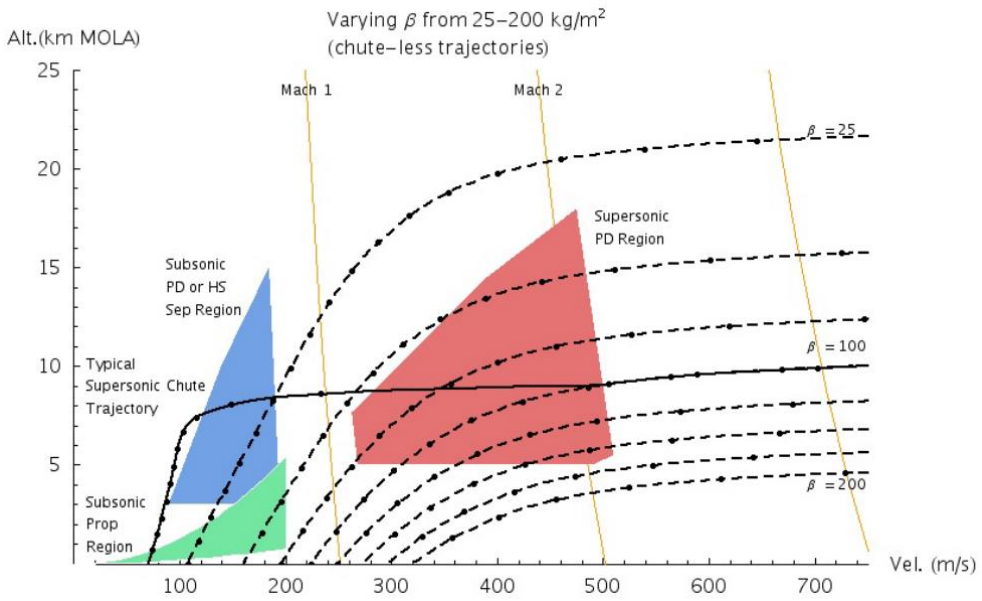

Figure 1. Vehicles with L/D = 0.18 and β > 150 kg/m^2 exceed the limits of current parachute technology.[3]

Supersonic retropropulsion provides an alternative method for descent and deceleration from supersonic speeds to soft landing. While multiple studies have examined the flight performance of SRP systems, none have examined the hypersonic trajectory required to reach an appropriate terminal descent initiation point for SRP systems. For vehicles using parachutes to decelerate from supersonic to subsonic speeds, altitude maximization is a useful objective function: additional altitude results in a longer descent and landing timeline, providing the parachute more time to slow the vehicle. However, altitude maximization is not clearly beneficial for SRP systems. Analyses of hypersonic flight to date have focused on maximizing altitude at terminal descent initiation at a given velocity. For vehicles using supersonic retropropulsion for terminal descent, the maximization of altitude at TDI is not an appropriate objective function—powered descent from high altitudes will incur significant gravity losses. Other objective functions may provide more beneficial results for EDL systems using supersonic retropropulsion.

The current state of the art in hypersonic trajectory control at Mars is the system used by the Mars Science Laboratory, which maintained a largely lift-up orientation but used control of the bank angle to decrease crossrange and downrange error.[3] Existing literature contains some information on optimizing hypersonic entry trajectories at Mars with bank angle control, but mostly with a focus on maximizing TDI altitude. Pritchard and Harrison studied the terminal descent initiation altitude benefits of lifting vehicles with low L/D assuming a fully lift-up orientation throughout flight.[4] García-Llama used optimal control to develop TDI altitude-maximizing references trajectories for an Apollo-derived controller.[5] Lafluer and Cerimele used a particle swarm optimization method to maximize TDI altitude for a range of entry vehicles at Mars, using both bank angle and angle of attack control.[6-7] Benito and Mease developed a computational approach to identify the sets of reachable landing states and controllable entry states for planetary entry vehicles using bank control, and used altitude-maximization to limit the size of the sets.[8] Johnson et al. minimized heat load and maximized cross range and down range for several bank-controlled Earth return vehicle geometries.[9] Other studies have also studied the minimization of heat load for entry trajectories.[10-11] Grant and Mendeck studied the tradeoff between maximizing TDI altitude, minimizing range error, and minimizing peak g-loading for the Mars Science Laboratory vehicle.[12] Lu developed optimal entry bank control laws for a variety of objective functions with applications to vehicles entering at Earth.[13]

Recently, Jacob et al. found TDI altitude-maximizing bank profiles for MSL class vehicles and studied the effect of varying ballistic coefficient and lift-to-drag ratio on TDI altitude and peak g-loading.[14] Anderson et al. also used optimal control to determine altitude-maximizing bank angle profiles for Mars entry with a focus on large ballistic coefficient vehicles.[15] This study adopts a more general approach, using multiple objective functions over a range of potential

vehicle parameters to assess the overall fitness of hypersonic flight strategies for EDL systems utilizing SRP.

CHAPTER 2: PROBLEM FORMULATION AND SOLUTION METHODOLOGY

A. Vehicle and Environmental Assumptions

This study focuses on high ballistic coefficient vehicles using a center-of-mass offset to generate lift. Vehicle parameters and atmospheric conditions have been identified that cover the likely range of vehicles for near-term robotic and human-precursor missions. A range of these vehicle and trajectory parameters have been chosen to span the vehicle and mission design trade space (see Table 1). This study focuses on optimizing trajectories in the presence of a set vehicle and atmospheric model, so landed accuracy due to dispersions is not considered. Hypersonic ballistic coefficient and lift-to-drag ratio are assumed to remain constant unless otherwise noted. All thrust-to-weight ratios are referenced to weight on the surface of Mars. For supersonic retropropulsion, a specific impulse of 300 s, corresponding to a storable pump-fed liquid bipropellant system, is assumed for all cases. All EDL simulations assume entry begins at 125 km above the Mars surface. EDL simulations terminate at a landed altitude of 0 km and a velocity at landing of 1 m/s unless otherwise stated.

Table 1. Minimum, Nominal, and Maximum Vehicle Parameters

Parameter	Minimum Value	Nominal Value	Maximum Value
Ballistic Coefficient (β)	150 kg/m^2	450 kg/m^2	600 kg/m^2
Lift-to-Drag Ratio (L/D)	0.10	0.24	0.30
Entry Interface Altitude (h_0)	—	125 km	—
Entry Interface Velocity (V_0)	5,000 m/s	5,845 m/s	7,500 m/s
Entry Interface Flight-Path Angle (γ_0)	-5 deg	-15.5 deg	-25 deg
TDI Velocity (v_f)	360 m/s	480 m/s	960 m/s
Thrust-to-Weight Ratio (T/W)	3	4	5

Acceleration due to gravity was assumed to be constant and an exponential model was used for atmospheric density, given by:

$$\rho = \rho_{ref} e^{\frac{(h_{ref}-h)}{H}} \tag{1}$$

Environmental constants for Mars are defined in Table 2.

Table 2. Environmental Parameter Assumptions

Parameter	Value
Reference Density (ρ_{ref})	0.02 kg/m^3
Reference Density Altitude (h_{ref})	0 km
Atmospheric Scale Height (H_{scale})	11.1 km
Speed of Sound	240 m/s
Radius of Mars (R_m)	3,390 km
Acceleration due to Gravity on Surface of Mars (g_m)	3.71 m/s^2
Acceleration due to Gravity on Surface of Earth (g_0)	9.81 m/s^2

B. Hypersonic Control Problem Formulation

Hypersonic flight from entry interface to terminal descent initiation has been formulated as an optimal control problem with a single control variable, the bank angle of the spacecraft, and a path-independent cost based on the terminal state. The planar equations of motion for a lifting body entering a planetary atmosphere are:

$$\begin{aligned} \frac{dV}{dt} &= \frac{\rho V^2}{2\beta} - g_m sin(\gamma) \\ \frac{d\gamma}{dt} &= \frac{V cos(\gamma)}{R_m + h} + \frac{\rho V}{2\beta}(L/D_{Max})u_1 - \frac{g_m cos(\gamma)}{V} \\ \frac{dh}{dt} &= V sin(\gamma) \end{aligned} \tag{2}$$

To maximize terminal altitude the cost is given in Mayer form:

$$J = -h_{TDI} \tag{3}$$

where h_{TDI} is the altitude at terminal descent initiation. The Hamiltonian of this system is:

$$H = p_V\left(\frac{\rho V^2}{2\beta} - g_m \sin(\gamma)\right) + p_\gamma\left(\frac{V cos(\gamma)}{R_m + h} + \frac{\rho V}{2\beta}(L/D_{Max})u_1 - \frac{g_m cos(\gamma)}{V}\right) + p_h\big(V sin(\gamma)\big) \tag{4}$$

The in-plane lift-to-drag ratio has been replaced by the maximum vehicle lift-to-drag ratio multiplied by the control variable $u_1 \in [-1,1]$. The control is related to the bank angle of the vehicle by:

$$u_1 = \cos(\sigma) \tag{5}$$

And the relationship between bank angle and vertical lift-to-drag ratio is shown in Figure 2.

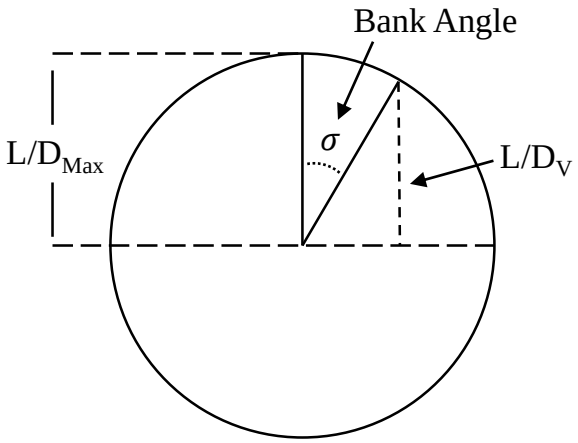

Figure 2. Geometry of vertical lift-to-drag ratio for a bank controlled vehicle.

The optimal solution can then be found using the Pontryagin Minimum Principle.[16] The Hamiltonian is linear in the control in Eq. 4, so the optimal control is bang-bang with the switching function given by:

$$S_1 = p_\gamma \frac{\rho V}{2\beta}(L/D_{Max}) \tag{6}$$

The sign of u is solely dependent on p_γ, since all other quantities in Eq. (6) are positive. The control will always be at its maximum magnitude (-1 or 1) to minimize the Hamiltonian. Terminal altitude may be substituted with alternative terminal vehicle by changing only the cost function, resulting no change to the formulation of the switiching function.

The terminal-altitude-maximization problem was solved numerically using the General Pseudospectral Optimization Software (GPOPS) package.[17] An example hypersonic trajectory solution is shown in Figure 3, where the altitude maximizing trajectory and control are coplotted with the open-loop case where the bank angle is constant at zero degrees in a lift-up orientation. The altitude-maximizing solution enters the atmosphere with the lift vector pointing down (bank angle of 180 deg) and performs a single switch to lift-up (bank angle of 0 deg) at approximately 80 seconds. The open-loop lift-up trajectory features a larger loft compared to the optimal solution before quickly losing altitude. Both trajectories terminate at a notinal parachute deploy point of 480 m/s (approximately Mach 2) with the lift-up case terminating at -2.3 km altitude and the altitude-maximized trajectory terminating at 3.2 km altitude. The altitude difference of 5.5 km is substantial in the context of Mars EDL systems. For example, MSL required just over 10 km for terminal descent; [18] an increase of 5.5 km may be enabling for some EDL systems. Altitude-optimal trajectories achieve higher TDI altitudes by diving deeper into the atmosphere, leading to

higher dynamic pressure and additional control authority earlier in the trajectory which allow the vehicle to maintain altitude longer. The optimality of this solution has been verified by inspection of the near-zero Hamiltonian and continuous costates of the problem, shown in Figure 4.

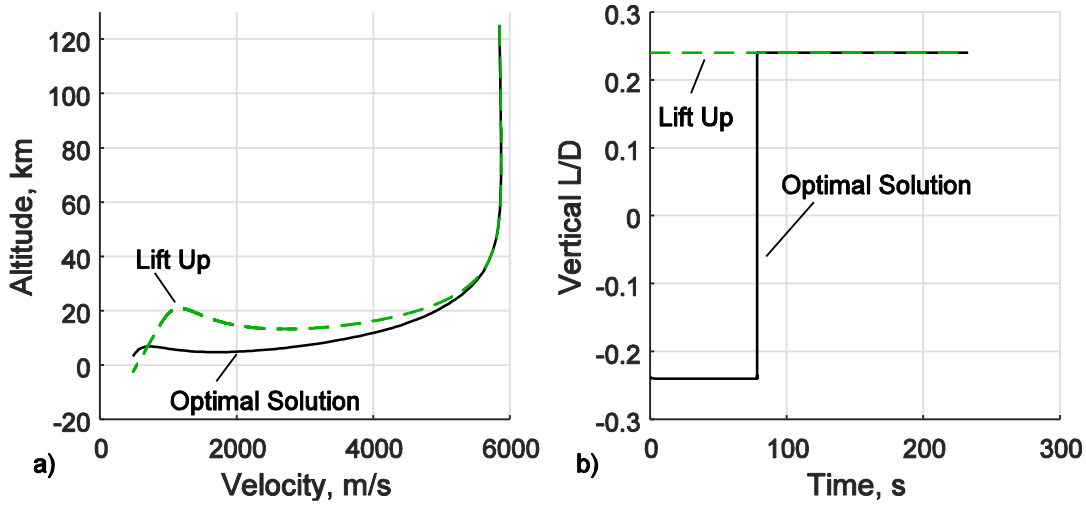

Figure 3. Example GPOPS solution for altitude maximization: a) trajectory and b) control profile.

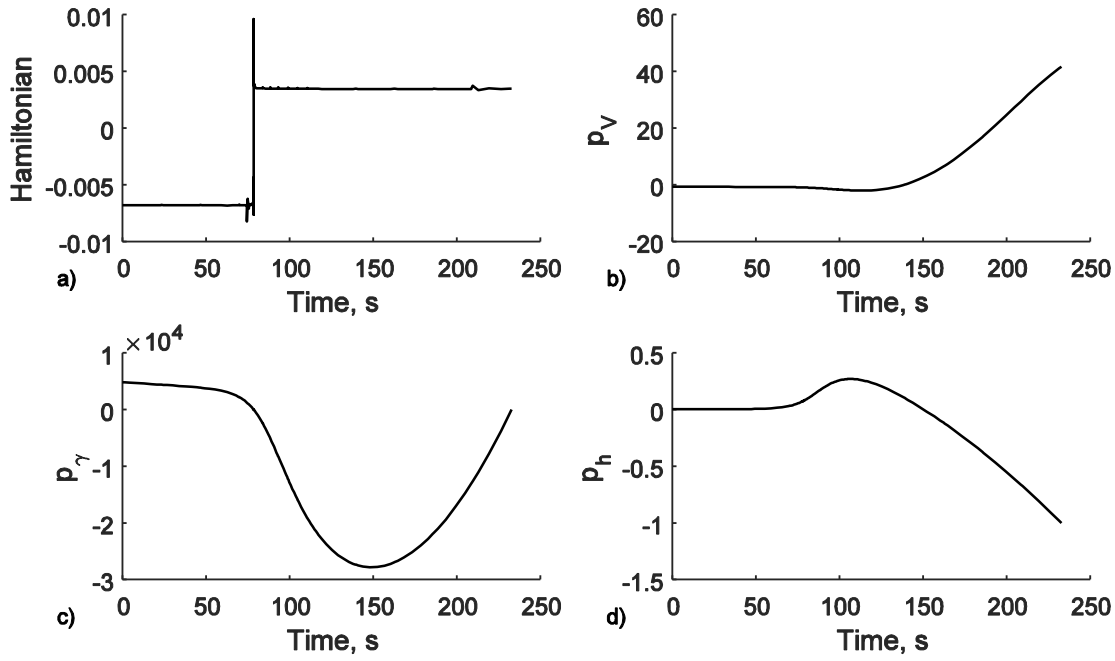

Figure 4. Hamiltonian and costates for the altitude maximizing optimal control problem.

C. Supersonic Retropropulsion Terminal Descent Problem Formulation

Following the hypersonic entry phase, the vehicle uses a supersonic retropropulsion system to eliminate remaining velocity and perform a soft landing on the surface of Mars. The supersonic retropropulsion steering strategy is a gravity turn, where the thrust direction is always opposite the velocity vector during propulsive descent. Gravity turn is not fuel optimal, but simplifies the analysis and provides near-optimal results for propellant mass.[19] This study assumes no aerodynamic drag preservation during the supersonic retropropulsion phase, a conservative assumption given that the presense of any drag would be benefical to deceleration performance and reduce required PMF. The equations of motion for SRP descent are:

$$\begin{aligned} \frac{dV}{dt} &= -g_m sin(\gamma) - Tu_2/m \\ \frac{d\gamma}{dt} &= \frac{Vcos(\gamma)}{R_m+h} - \frac{g_m cos(\gamma)}{V} \\ \frac{dh}{dt} &= Vsin(\gamma) \\ \frac{dm}{dt} &= -\frac{Tu_2}{g_0 I_{sp}} \end{aligned} \tag{7}$$

where, $u_2 \in [0,1]$ is the throttle control parameter. These equations are similar to Eq. (2), but with the aerodynamic force terms removed and the addition of the mass state and a thrust term in the velocity derivative. Minimizing the total mass of the landing system allows a larger payload to be carried, so for a supersonic retropropulsion system the minimization of required propellant mass is a useful figure of merit:

$$J = -m_f \tag{8}$$

where m_f is the vehicle mass at touchdown. The vehicle propellant mass fraction (PMF) is used to quantify the performance of the SRP system and is defined as:

$$PMF = 1 - \frac{m_f}{m_0} \tag{9}$$

The Hamiltonian for propulsive descent is:

$$H = p_V\left(-g_m \sin(\gamma) - \frac{Tu_2}{m}\right) + p_\gamma\left(\frac{V cos\gamma}{R_m + h} - \frac{g_m cos\gamma}{V}\right) + p_h(V sin\gamma) - p_m\left(\frac{Tu_2}{g_0 I_{sp}}\right) \tag{10}$$

Again, the optimal control for powered flight is bang-bang. The switching function is given by:

$$S_2 = -p_v\frac{T}{m} - p_m\frac{T}{g_0 I_{sp}} \tag{11}$$

A two-phase optimal control problem was formulated, where the first phase is gliding, hypersonic flight, as formulated in Section II.B, and the second phase is powered descent using supersonic retropropulsion with an initial thrust-to-weight of 4. The cost function for the two-phase problem was the SRP phase cost in Eq. 7. Thrust-to-weight is defined using the weight of the vehicle under Mars surface gravity. The phase switch time was left free and a constraint was placed on the system such that states before and after the switch between phases must be equal;

instantaneous changes in state derivatives were allowed between phases. Figure 5 shows the resulting trajectory and control for both phases of the optimal control problem.

Figure 4 shows a hypersonic control history similar to that of the altitude maximizing case, where the control begins lift-down until a single switch is made to lift-up. Since no drag is modelled in the SRP phase of flight, the optimizer switches to the powered-flight phase at the latest time possible while still landing successfully, thereby maximizing the deceleration effect of atmospheric drag experienced prior to ignition. Terminal descent is performed at full throttle to minimize gravity losses during descent.

The Hamiltonian and costates for both phases of this example optimal control problem are shown in Figure 6. The Hamiltonian is near-zero with smooth costates for both phases of the trajectory, verifying the optimality of the solution.

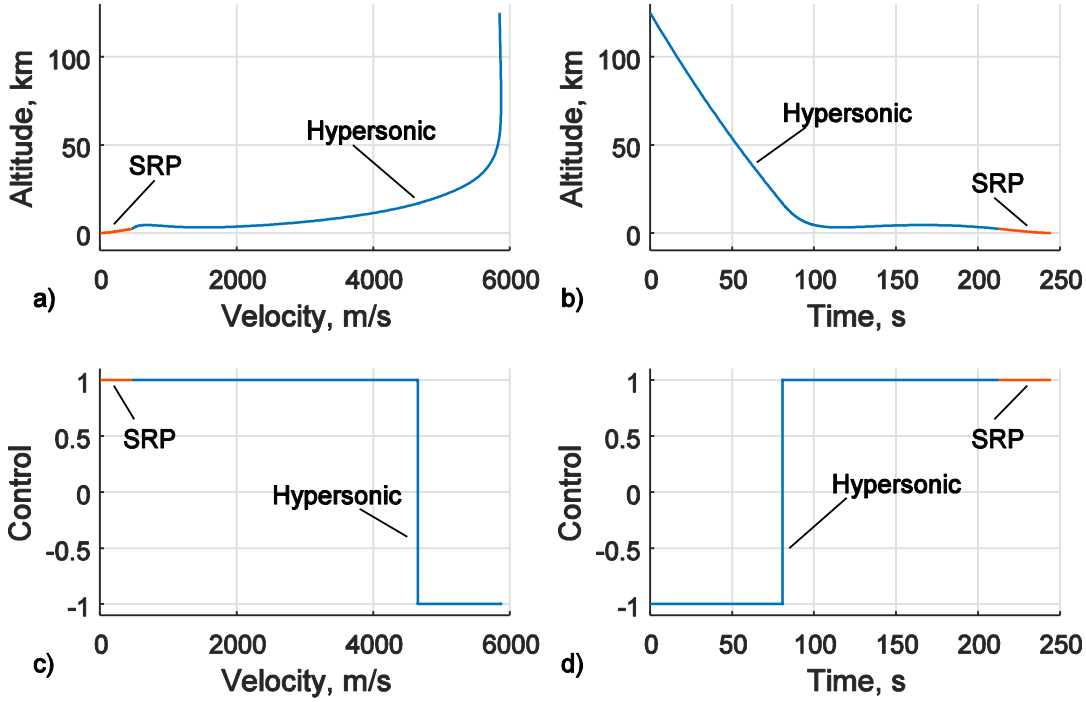

Figure 5. Full trajectory in the velocity domain (a) and time domain (b), optimal control in velocity domain (c) and time domain (d).

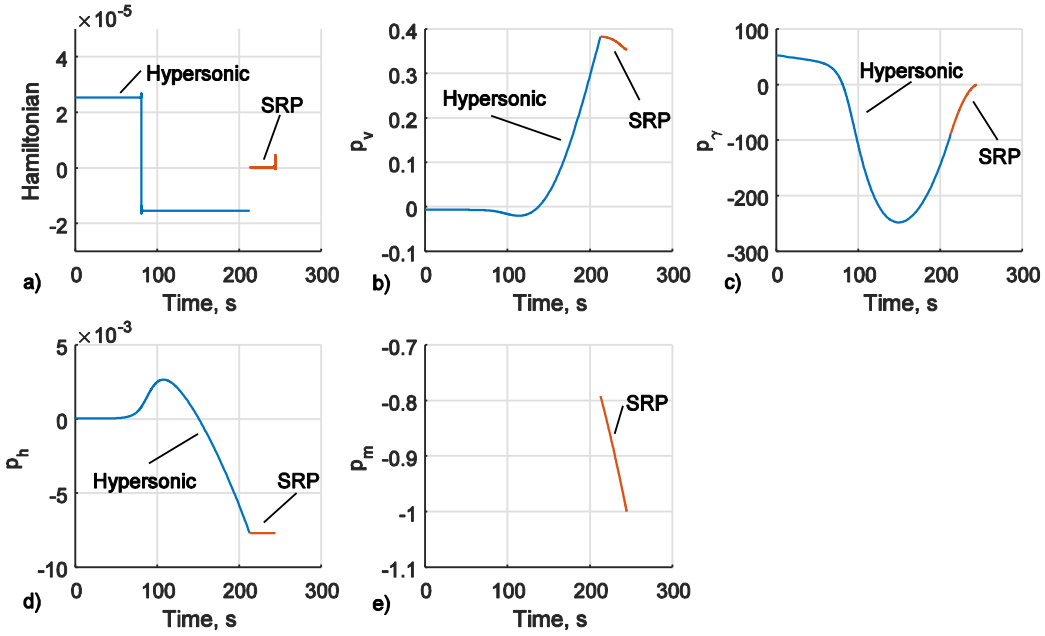

Figure 6. Hamiltonian and costates for the two-phase problem.

CHAPTER 3: RESULTS

A. TDI Altitude Maximization Solution Validation

Higher-fidelity vehicle and environment models were used to verify that optimal control solutions for the problems described above are valid under more realistic conditions. Mach-dependent lift and drag coefficients from the Mars Phoenix capsule at an angle of attack of 16 deg were used as a more accurate model for vehicle aerodynamics.[20] Bank acceleration was constrained to ±5 deg/s^2; bank rate was limited to ±10 deg/s. An altitude-dependent inverse square gravity model was used. Atmsopheric density was modeled with the Mars Global Reference Atmospheric Model (MarsGRAM).[21]

This higher-fidelity case is compared to the previous altitude-maximizing bang-bang control solution case in Figure 7. While there are significant differences in the maximum altitude of the trajectory and the time of the switch from lift-down to lift-up, these stem from changes in vehicle aerodynamic properties and the atmospheric density profile. The structure of the solution, both the shape of the trajectory and the overall switching nature of the bank angle, is preserved.

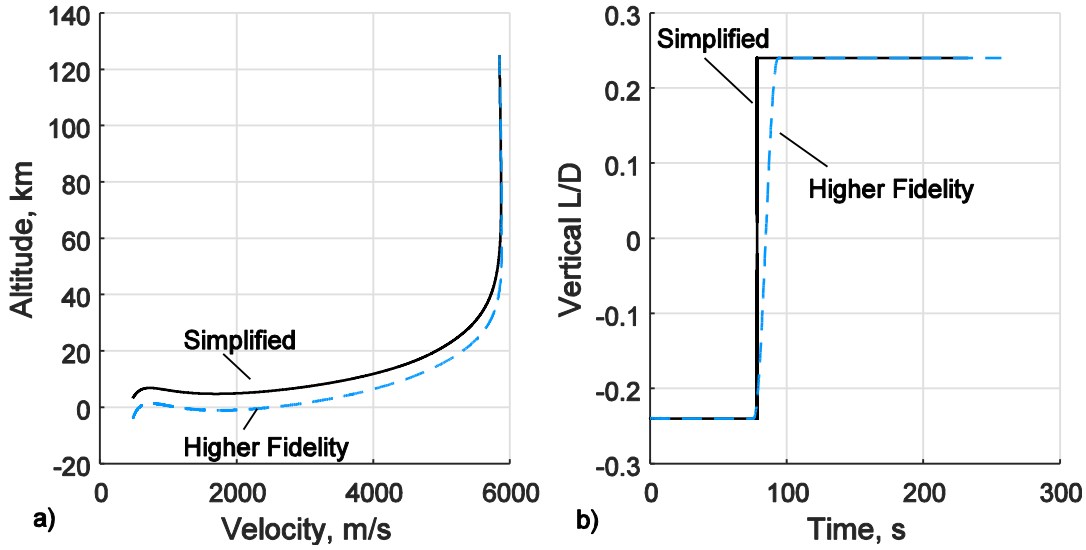

Figure 7. Trajectory in altitude velocity space (left) and control history (right) for the bang-bang and rate limited cases.

The optimality of solutions produced by these models has been verified by observation of the small magnitude of the Hamiltonian and the continuity of the costates (see Figure 8). The elimination of constraints on the bank angle rate and the simplified vehicle and atmosphere models greatly reduce computation time and solution stability, so the simplified case is used for the rest of this study.

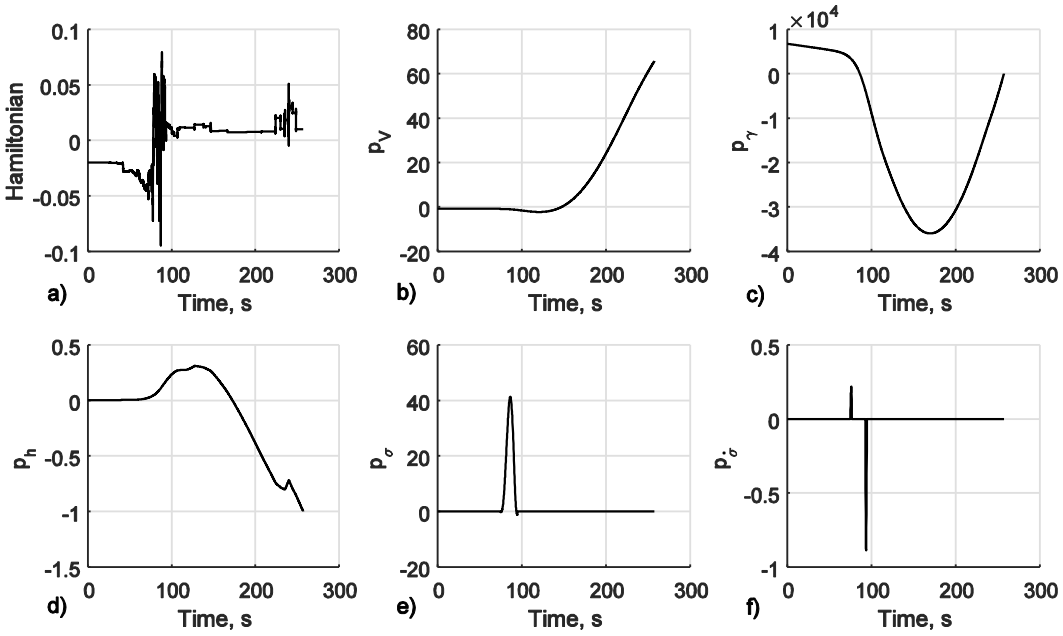

Figure 8. Hamiltonian and costates for the example solution using higher-fidelity models.

B. TDI Altitude Maximization Control Profiles

TDI altitude was maximized for the nominal vehicle (see Table 1) over a range of entry interface velocities (5,000 to 7,500 m/s) and entry interface flight-path angles (-5 to -25 degrees). Results are shown in Figure 9. The highest TDI altitudes are found at high initial velocities and steeper initial flight-path angles. These trajectories are optimal only from a TDI altitude perspective and do not take into account constraints due to cumulative heat load or maximum acceleration.

The red lines in Figure 8 show the location of the boundaries between no switch, one switch, and skip out trajectories. Entry states in the "1 Switch" region result in control histories similar to the optimal solution in Figure 3, where the vehicle begins lift-down and then at an optimal point flips to the full lift-up position. Single-switch trajectories allow the vehicle to spend

more time deep within the atmosphere decelerating, allowing the vehicle to reach the same TDI velocity at a higher altitude relative to lift-up trajectories. Entry states in the "No Switch" region are trajectories where the optimal control history is purely lift-up. "Skip out" trajectories do not decelerate sufficiently to remain within the atmosphere, even with full lift-down bank profiles.

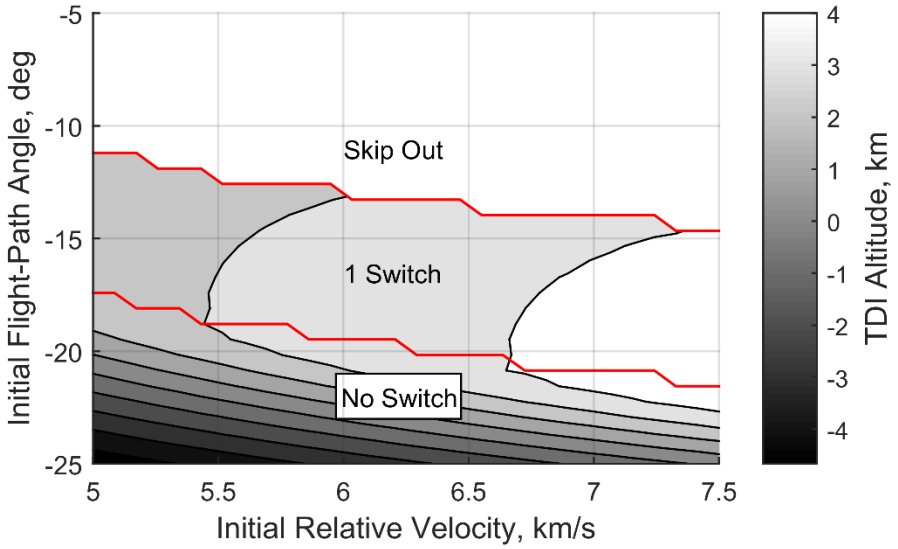

Figure 9. Maximum altitude at TDI over a range of entry conditions with the lift-up boundary shown in red.

The location of the lift-up boundary is key to determining the ideal type of control profile for a given vehicle configuration and entry state. This boundary shows the entry trajectory designer what nominal control profile is likely to produce maximum TDI altitudes. The location of this boundary was identified for a range of vehicle ballistic coefficients, lift-to-drag ratios, and terminal descent initiation velocities over the same space of entry states. Figure 10 shows the variation of this boundary for a range of ballistic coefficients from 150 kg/m^2, corresponding to Mars Science Laboratory, to 600 kg/m^2, an estimate of the upper bound for near-term, large-scale robotic missions, such as a Mars sample return and human precursor missions.[22] Three past missions are

included for context: Mars Pathfinder (MPF), the Mars Exploration Rovers (MER), and the Mars Science Laboratory (MSL). While these trajectories are not identical, there is little variation in the location of the boundary across this range of ballistic coefficients.

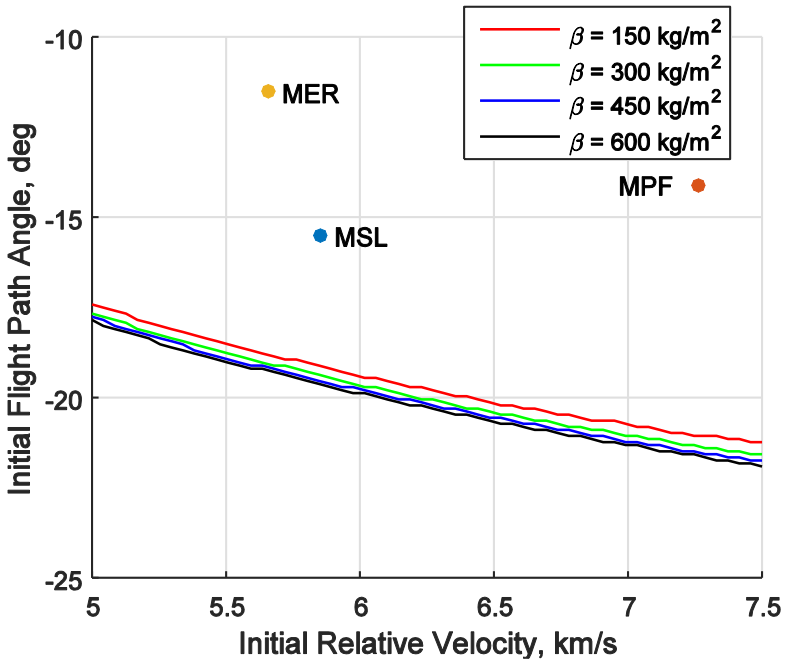

Figure 10. Location of the lift-up boundary for several ballistic coefficients.

Lift-to-drag ratio has a strong effect on the location of the lift-up boundary. Control strategy boundaries for L/D varying from 0.10 to 0.30 are shown in Figure 11. Vehicles with the greater control authority offered by larger L/D can better take advantage of a bang-bang control scheme to achieve higher TDI altitudes for a wider range of entry conditions. Low L/D vehicles are better suited to a purely lift-up control strategy, as they require all of their lift control authority to pull the vehicle out of its initial entry dive.

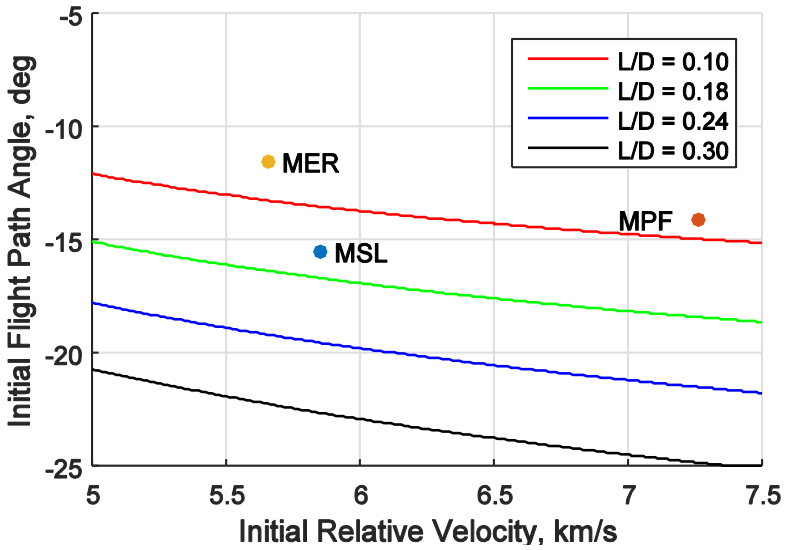

Figure 11. Location of the lift-up boundary for several lift-to-drag ratios.

TDI velocity was varied to determine its effect on the boundary. The TDI velocity was varied between Mach 1.5 and 4.0 and the boundary locations can be seen in Figure 12. Lesser terminal Mach numbers are generally more desirable for both parachute and propulsive descent systems. For propulsive systems, the propellant required to decelerate fully and land can be significantly decreased. For parachute systems, dynamic pressures are lower and Earth-based testing is simplified for lower Mach numbers. Vehicles beginning terminal descent at these lesser Mach numbers benefit from the bang-bang controller over a wider range of initial conditions than vehicles at greater Mach numbers.

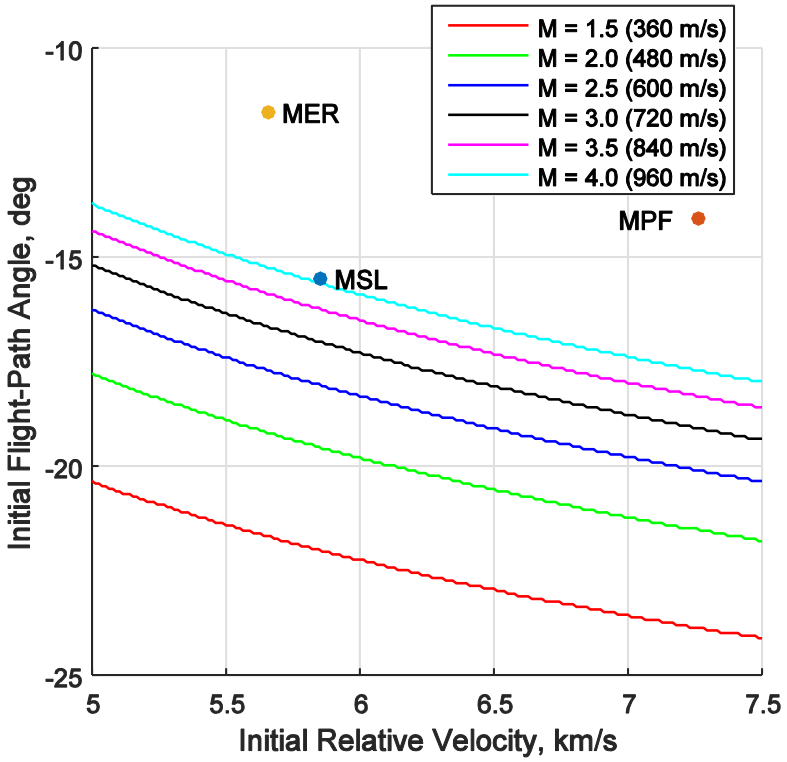

Figure 12. Location of the lift-up boundary for several TDI Mach numbers.

C. Peak Acceleration Limits for TDI Altitude Maximizing Trajectories

Acceleration experienced during flight determines the mass of structure required to support the vehicle through entry. Additional requirements are placed on acceleration for crewed missions to protect the humans onboard. The Human-Systems Integration Requirements document developed as a part of NASA's Constellation Program gives duration-based acceleration limits for crewed vehicles.[23] Compliance with these conditions was checked for TDI-altitude-maximizing trajectories to determine what portion of the space in Figure 9 meets acceleration limits for humans and robotic missions. These results are shown in Figure 13, with the acceleration values given in terms of Earth g's. Points above and to the left of the constraint lines fall below the given g-load

values, while the points below and to the right exceed these values. The HSIR limit is based on the maximum allowable acceleration upon Earth return for ill/deconditioned crew in the +X eyeballs-in direction.

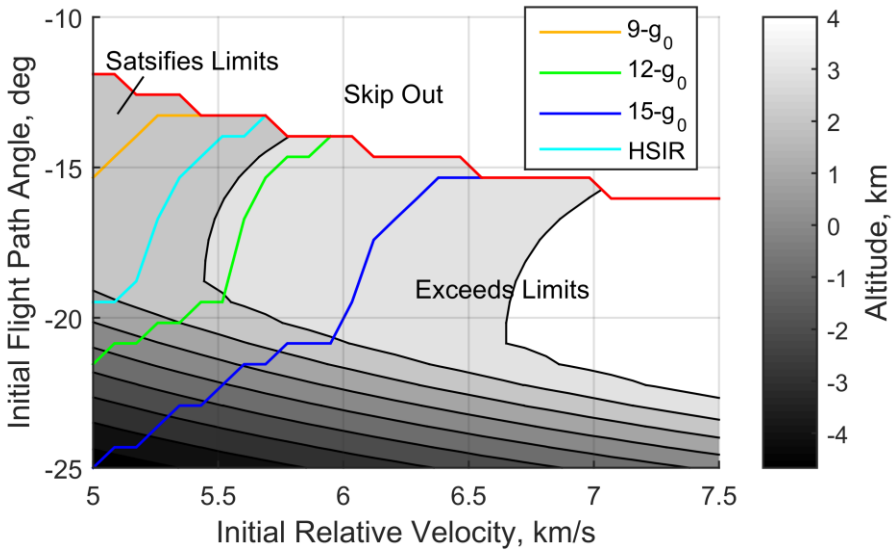

Figure 13. TDI altitude maximizing trajectories satisfying acceleration requirements.

Low entry velocities and shallow entry flight-path angles decrease the maximum acceleration values encountered during entry. A tradeoff exists between maximizing altitude through increased entry velocity and steeper flight-path angles and limiting peak deceleration.

D. TDI Altitude Maximization with Constrained TDI Flight-Path Angle

Higher TDI altitudes provide more timeline margin and the ability to land at higher surface altitudes. This is beneficial for some architectures including parachute-based descent systems, but for vehicles utilizing supersonic retropropulsion, minimization of propellant mass fraction is a more relevant figure of merit for maximizing landed payload mass.

Higher altitudes at a given terminal velocity are not necessarily beneficial, as supersonic retropropulsion descent is completed in a much shorter timeframe than parachute descent. Past work by Korzun and Braun has shown that shallower TDI flight-path angles lead to lower propellant mass fractions by reducing gravity losses during descent.[1] While targeting TDI flight-path angles near zero degrees reduces propellant mass fraction, purely maximizing flight-path angle typically yields TDI altitudes below the desired landed altitude. To explore the possibility of minimizing TDI flight-path angle, performance with a TDI flight-path angle constraint was evaluated. The TDI velocity was held constant and the terminal flight-path angle constraint was varied. As seen in Figure 14, this results in a direct tradeoff between TDI altitude and flight-path angle. The set of maximum achievable TDI altitudes at constrainted TDI flight-path angles is a Pareto frontier. The Pareto frontier in Figure 14 can be used to identify the shallowest flight-path angle attainable for a given TDI velocity while still remaining above a given altitude. The TDI state space above these contours is unreachable for the given vehicle.

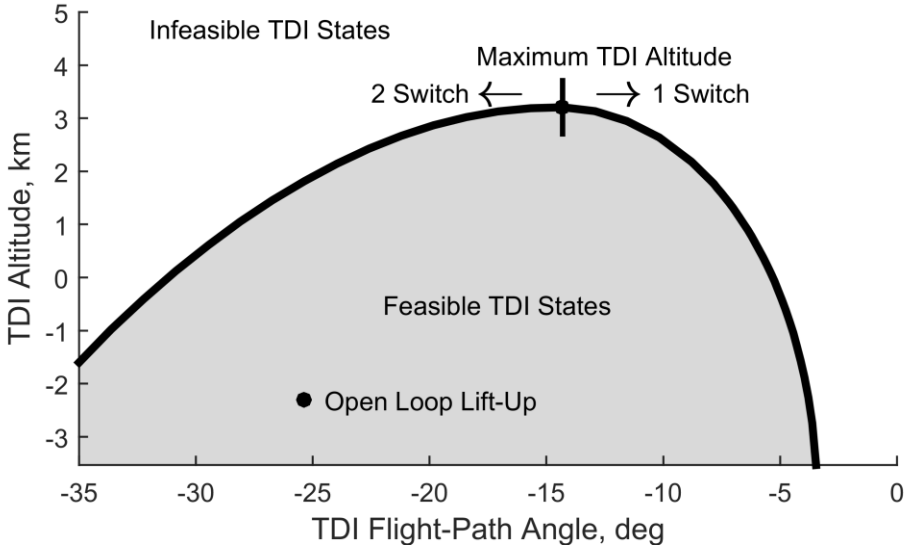

Figure 14. Terminal descent initiation altitude with a flight-path angle constraint.

This Pareto frontier provides an insight into the tradeoff for one specific case; in general, the curve will shift as vehicle parameters or terminal velocity are varied. For the majority of cases, trajectories to the right of the maximum altitude on a given Pareto frontier (shallower TDI flight-path angles) follow the same single switch pattern as the altitude maximizing cases: they enter the atmosphere lift-down and switch to lift-up at a given point, with the point varying in time to create the curve shown. Cases to the left (steeper TDI flight-path angles) of the maximum altitude case rely on a two switch control, where they begin lift-down and transition to lift-up at a given point, but then switch back down to lift-down just prior to TDI. An example of this is shown in Figure 15 for shallow (-10 deg) and steep (-25 deg) TDI flight-path angles. The location of both of these switch points varies based on the specific trajectory properties.

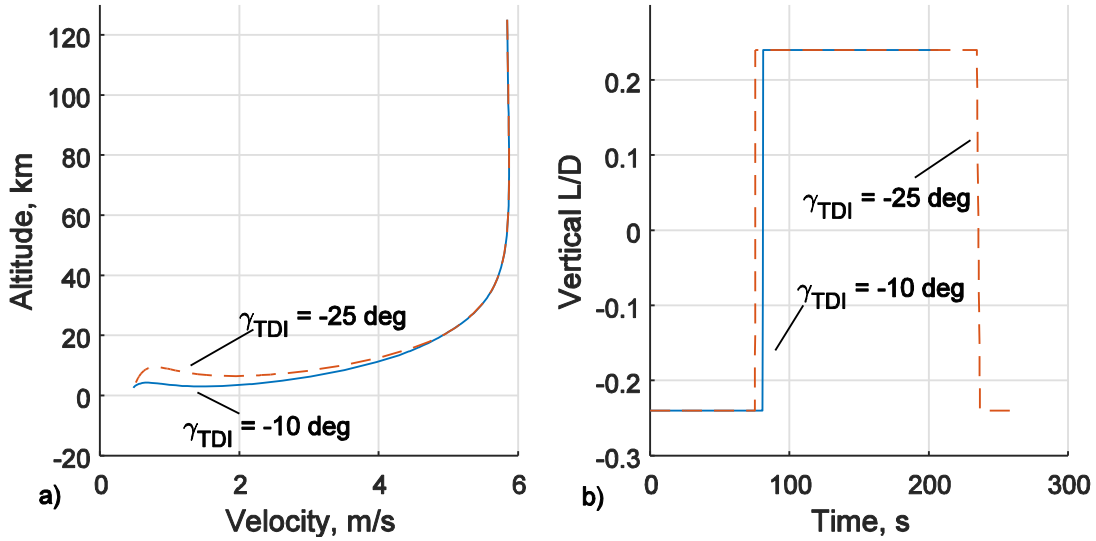

Figure 15. Trajectories (a) and control histories (b) for vehicles maximizing TDI altitude while constrained to -10 and -25 deg TDI flight-path angles.

The same analysis was applied to a variety of cases where the ballistic coefficient, lift-to-drag ratio, and terminal descent initiation velocity were each varied independently and is shown

in Figure 16. Larger ballistic coefficients decrease the achievable altitudes for the vehicle with no major effect on the possible flight-path angles. Increasing lift-to-drag ratio allows vehicles to reach a wider range of TDI flight-path angles at higher altitudes. Initiating terminal descent at a higher Mach number allows the vehicle to begin the final phase of descent at a higher altitude. As terminal descent initiation Mach number decreases, steeper TDI flight-path angles are seen as the vehicle moves farther past the lofting phase of flight.

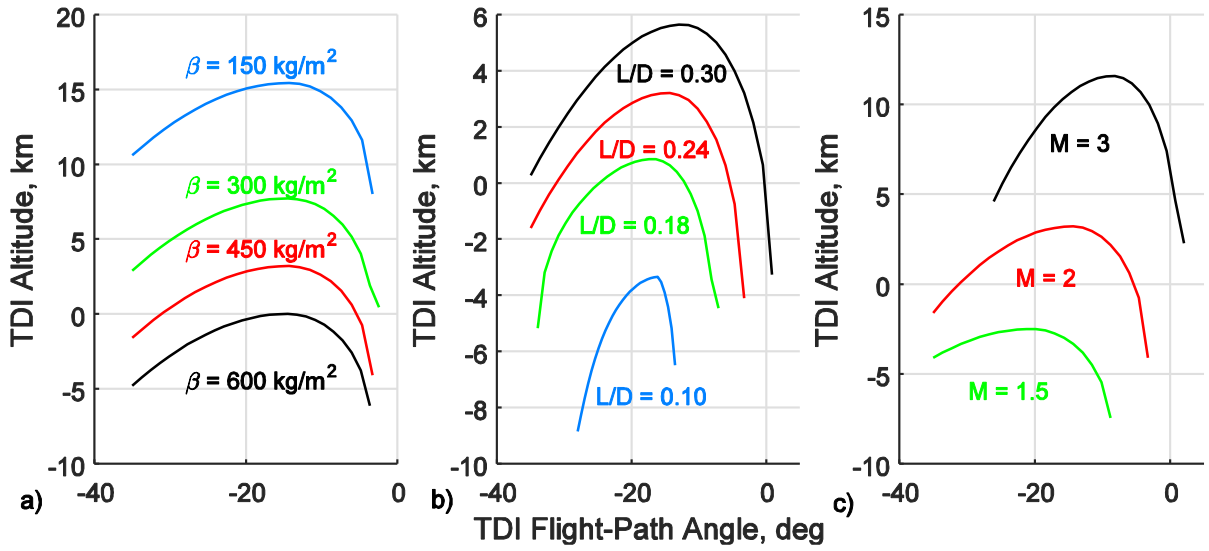

Figure 16. Terminal descent initiation flight-path angle constraint applied to various ballistic coefficients (a), lift-to-drag ratios (b), and TDI Mach numbers (c).

E. Propellant Mass Fraction Minimization

Supersonic retropropulsion PMF was minimized over a range of entry conditions and vehicle parameters to determine how these parameters affect minimum PMF. Figure 17 shows minimum PMF as a function of ballistic coefficient (a), entry flight-path angle (b), lift-to drag-ratio (c), and entry velocity (d). Smooth trends can be observed for all cases except ballistic coefficient, which flattens out below 250 kg/m^2 due to a Mach 1.5 lower bound on TDI. The lower

bound on Mach number at TDI avoids flight conditions where a 70 degree sphere-cone capsule at a 16 degree angle of attack (similar to MSL) loses much of its aerodynamic drag and static stability.[13]

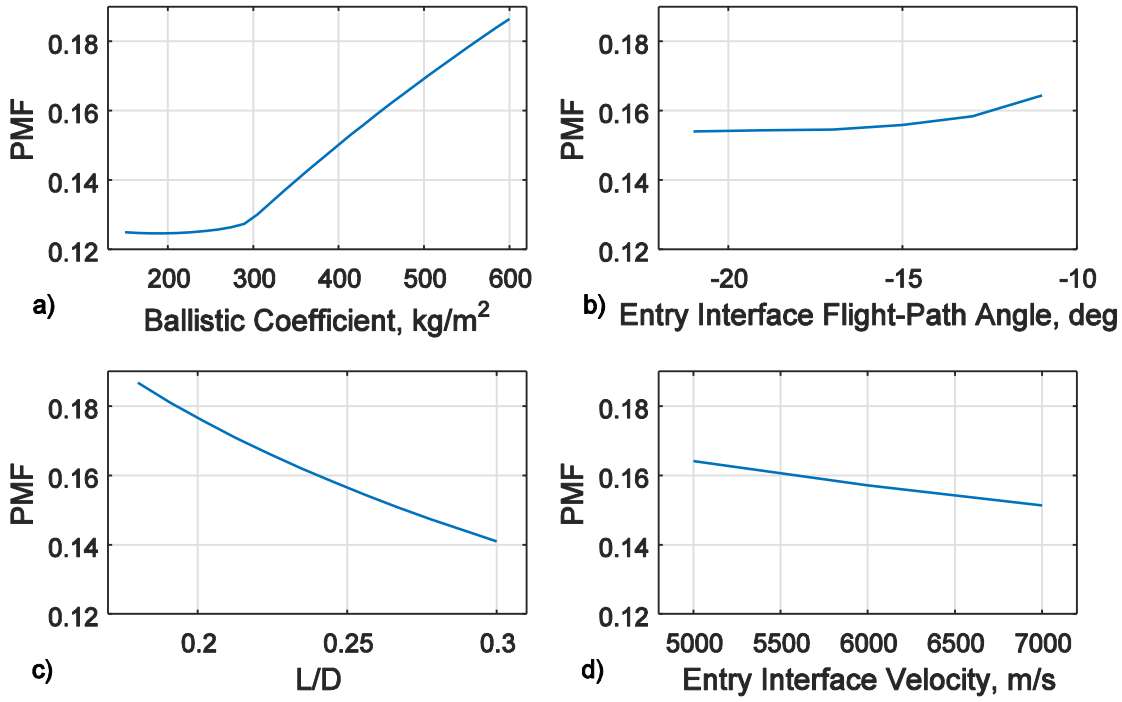

Figure 17. Results of minimum PMF trajectories as a function of a) ballistic coefficient, b) entry interface flight-path angle, c) lift-to-drag ratio, and d) entry interface velocity.

Ballistic coefficient and lift-to-drag ratio have a larger effect on PMF than entry interface conditions over the range of parameters studied. Vehicles with a lower ballistic coefficient and higher lift-to-drag ratio provide the ability to reach significantly lower PMFs. Steeper entry interface flight-path angles and faster entry interface velocities provide the ability to reach the surface with a smaller PMF. By entering steeper, faster, or both, the vehicle dives deeper into the atmosphere, increasing control authority of the relatively low-L/D system. While this analysis shows that large entry interface velocities and steep entry interface flight-path angles are beneficial

from a PMF perspective, a trade off exists between this decreased PMF and the increased vehicle mass due to additional structure support and thermal protection needed to survive a more stressful aerothermal environment.

F. Reachable Supersonic Retropropulsion Initiation States

To minimize PMF, a vehicle should fly hypersonically to the TDI state corresponding to the minimum PMF as described in the section above. However, in a realistic system, uncertainties in vehicle and atmospheric properties will prevent such precise targeting of a TDI state. It is therefore of relevance to determine the range of TDI states that the vehicle can reach from entry interface over vehicle and mission design parameters of interest.

Given the three TDI states of this dynamical system (velocity, flight-path angle, and altitude), for a given choice of entry interface velocity and flight-path angle and landed altitude, there exists a single altitude at which it is PMF-optimal to begin supersonic retropropulsion terminal descent using a gravity turn steering scheme. This TDI altitude corresponds to the minimum altitude at which the supersonic retropropulsion system can be ignited and still slow the vehicle to near-zero velocity before reaching the surface. Any TDI state prior to this altitude will increase the required PMF by decreasing the effectiveness of drag deceleration or increasing burn time and gavity losses. Any TDI state after this optimal initiation point will not have sufficient time to slow to zero velocity at the prescribed thrust level and will impact the surface. This altitude can be identified for any choice of TDI velocity and flight-path angle, leaving a two-dimensional surface of PMF-optimal supersonic retropropulsion initiation points. Each of these points also corresponds to a single PMF required to slow the vehicle from TDI velocity to zero velocity at the surface. The altitude (blue) and PMF (grayscale) contours for a set of TDI velocities and flight-path angles are shown in Figure 18. These points were obtained assuming a supersonic

retropropulsion system with a nominal initial thrust-to-weight ratio of 4 and a specific impulse of 300 s. The mass of the vehicle decreases as the supersonic retropropulsion system burns, but the thrust remains constant, leading to an increase in T/W over the burn.

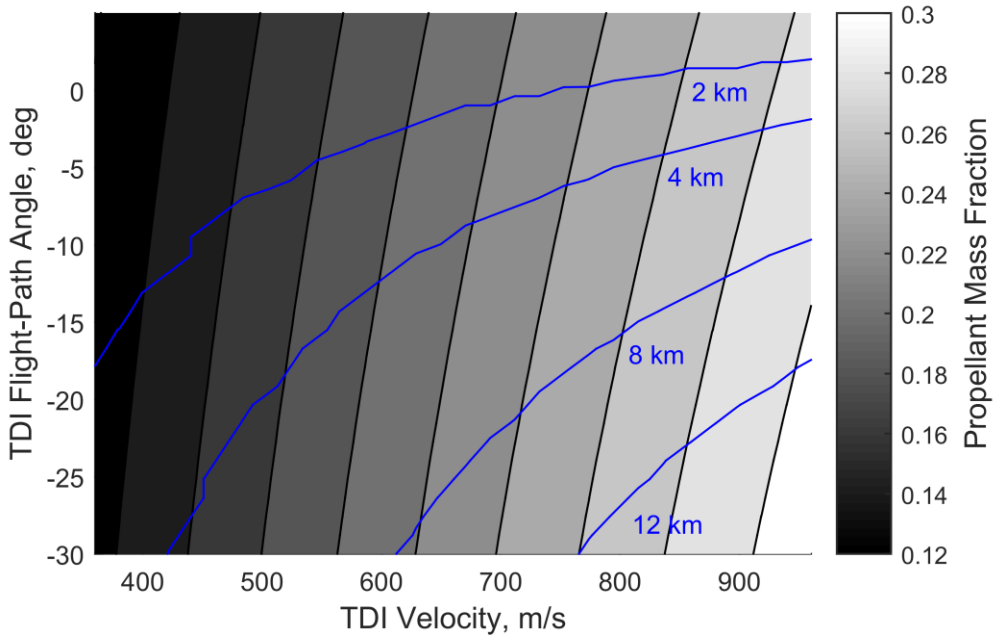

Figure 18. TDI altitudes from which gravity turn descent in PMF-optimal.

The shaded contours of propellant mass fraction on the plot in Figure 16 show a consistent dependence on both TDI flight-path angle and velocity. As TDI velocity decreases, a sharp decrease in PMF is observed. TDI flight-path angle has a smaller effect, but as the flight-path angle becomes more shallow, the vehicle PMF also decreases.

Each point in Figure 18 corresponds to a potential PMF-optimal terminal descent initiation state. However, not all of these TDI states are reachable using hypersonic control for a given vehicle and entry interface state. Each point was targeted using hypersonic control to determine

which states are achievable. A vehicle with a ballistic coefficient of 450 kg/m^2 and a lift-to-drag ratio of 0.24 with the same atmospheric conditions described in Table 1 was used.

The optimal control problem used a similar formulation to the hypersonic altitude maximization problem with a different cost function. The cost function for this problem is a minimization of the squares of the normalized differences between the final state achieved and the goal TDI state:

$$J = \left(\frac{V_{TDI} - V_{goal}}{V_{goal}}\right)^2 + \left(\frac{\gamma_{TDI} - \gamma_{goal}}{\gamma_{goal}}\right)^2 + \left(\frac{h_{TDI} - h_{goal}}{h_{goal}}\right)^2 \quad (12)$$

The space of flight-path angles was chosen to avoid infinite values of the second term of the cost. A threshold on the cost was set to 10^{-3} and any trajectory exceeding this cost was considered to be infeasible. Figure 19 shows the result of this analysis, where all of the points within the red outlined region are reachable hypersonically for the given conditions.

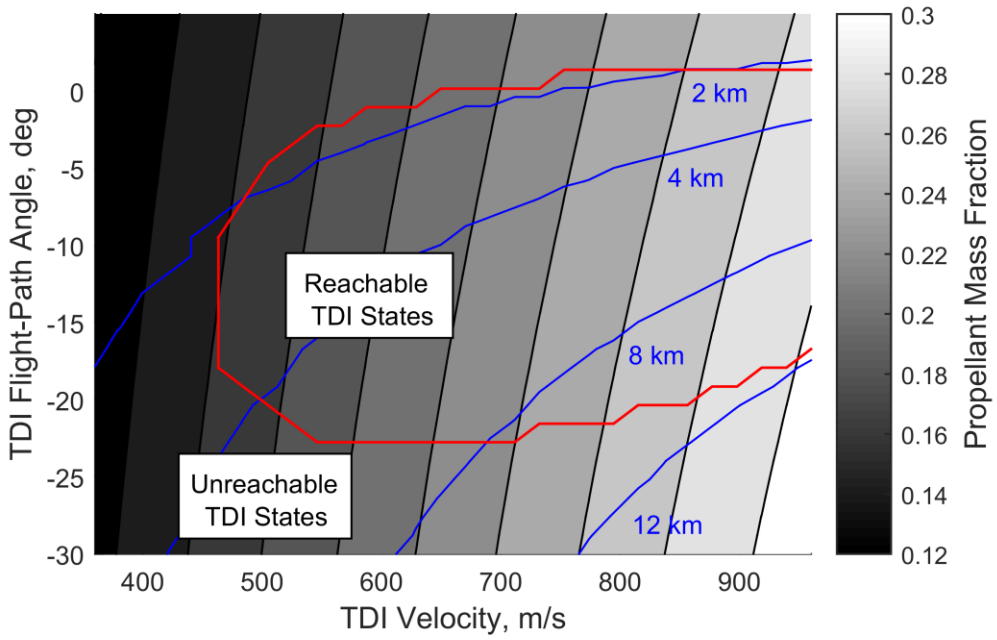

Figure 19. Reachable TDI states for a given vehicle configuration.

Based on this analysis, the minimum-PMF trajectory is located at the left of the reachable space at the minimum achieveable TDI velocity, which for this vehicle configuration has a PMF of approximately 0.16. This technique can be repeated for a range conditions to highlight the extent and range of reachable conditions for a set of vehicle configurations.

Applying this method over the range of ballistic coefficients in Table 1 yields the reachable regions shown in Figure 20. Lower ballistic coefficients allow for greater atmospheric drag during descent and therefore lower TDI velocities and lower PMFs. Vehicles with low ballistic coefficients are also incapable of initiating TDI at shallow flight-path angles for the low altitudes along this supersonic retropropulsion surface, since the vehicle must fly deeper in the atmosphere to meet these conditions. This is clear from the shift towards steeper TDI flight-path angles in the hypersonic reachable space as ballistic coefficient decreases.

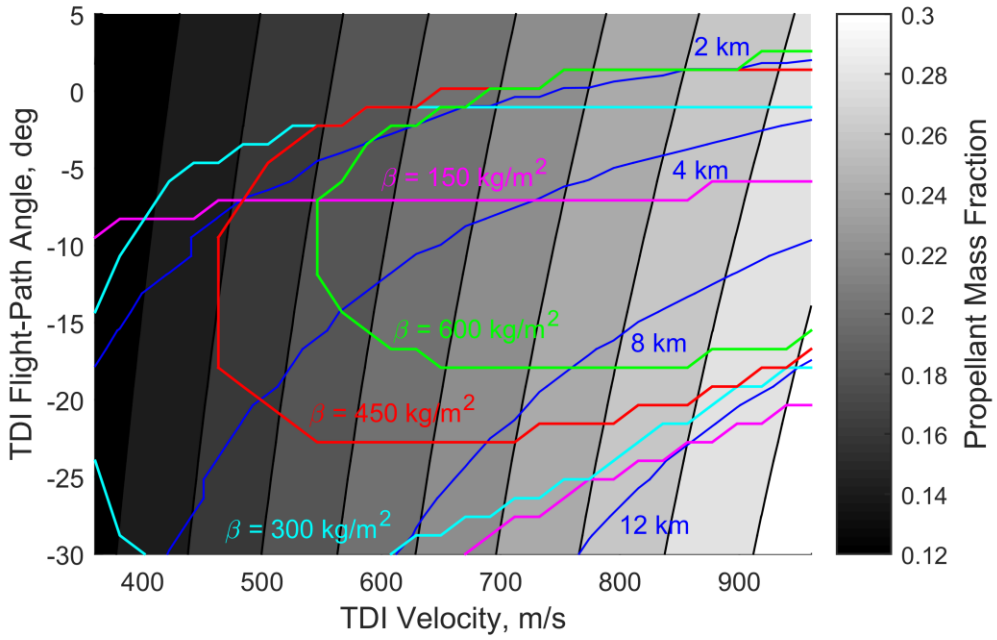

Figure 20. Reachable TDI states for several ballistic coefficients.

A larger lift-to-drag ratio enables an increase in the size of the reachable space of SRP initiation points and potential decrease in vehicle PMF as seen in Figure 21. A mass tradeoff therefore exists between increasing L/D in the hypersonic portion of flight and decreasing PMF in the supersonic region. Lift-to drag ratio has a significant effect on minimum PMF, in agreement with Figure 17, as well as on the size of the reachable TDI state space.

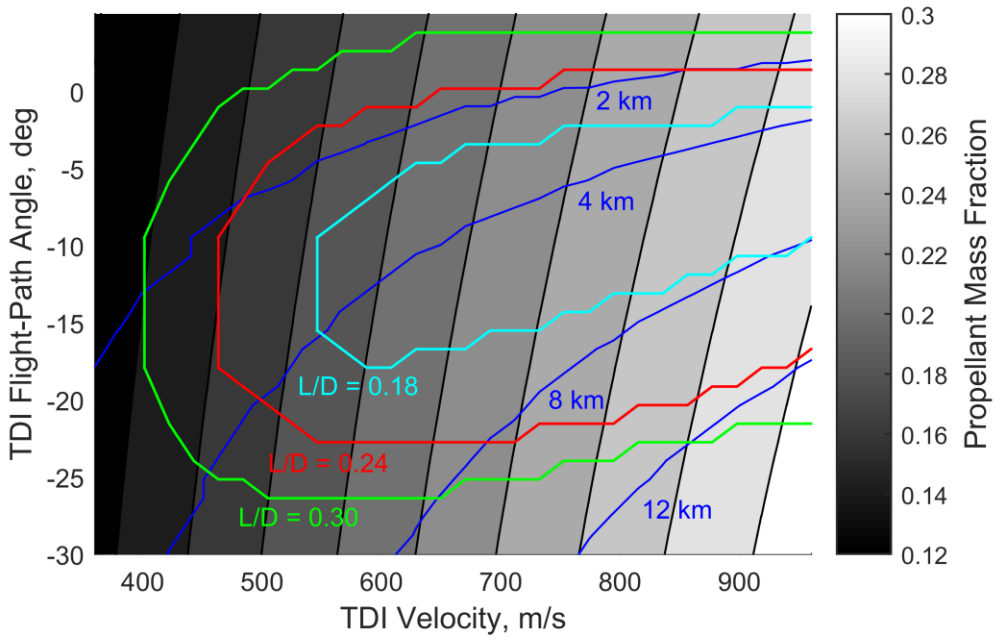

Figure 21. Reachable TDI states for several hypersonic lift-to-drag ratios.

The entry interface velocity of the vehicle has a similar but smaller effect than lift-to-drag ratio over the range of TDI conditions. As the entry velocity increases, the size of the reachable region grows and lower PMFs are achievable, as shown in Figure 22. As entry velocity increases, so does the control authority available to the vehicle during entry, enabling the vehicle to reach a larger set of TDI states.

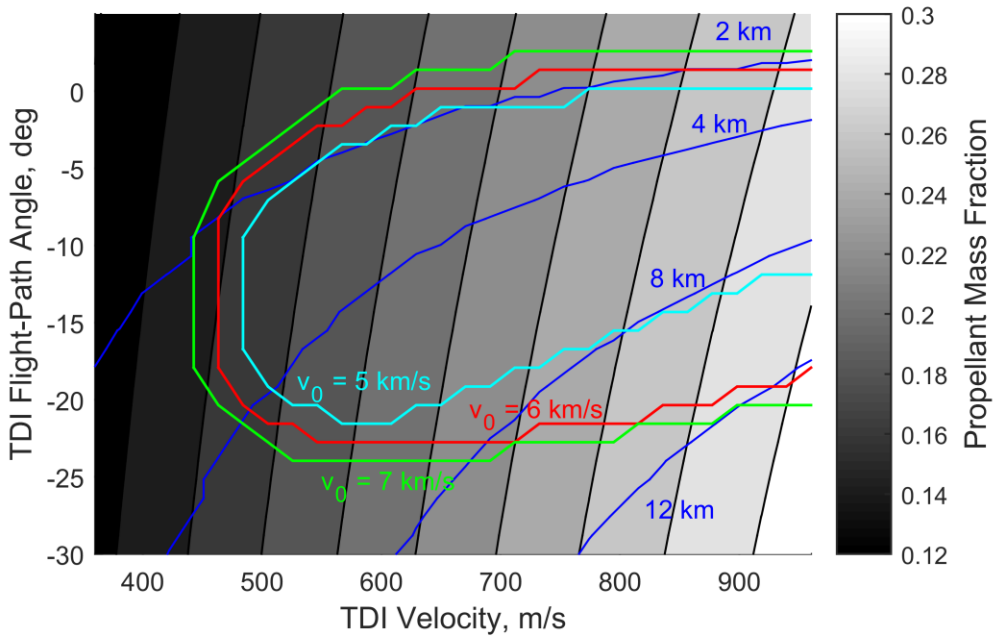

Figure 22. Reachable TDI states for several entry velocities.

Entry flight-path angle was also varied over a wide range of potential angles in Figure 23. As the entry flight-path angle gets steeper, lower PMFs are achievable. Beyond -15 degrees the space begins to shrink as the vehicle is unable to reach the required TDI velocities with sufficient altitude. Initial flight-path angles significantly steeper than -21 deg result in no reachable TDI states, meaning supersonic retropropulsion landing is infeasible for those specific initial states and vehicle configurations.

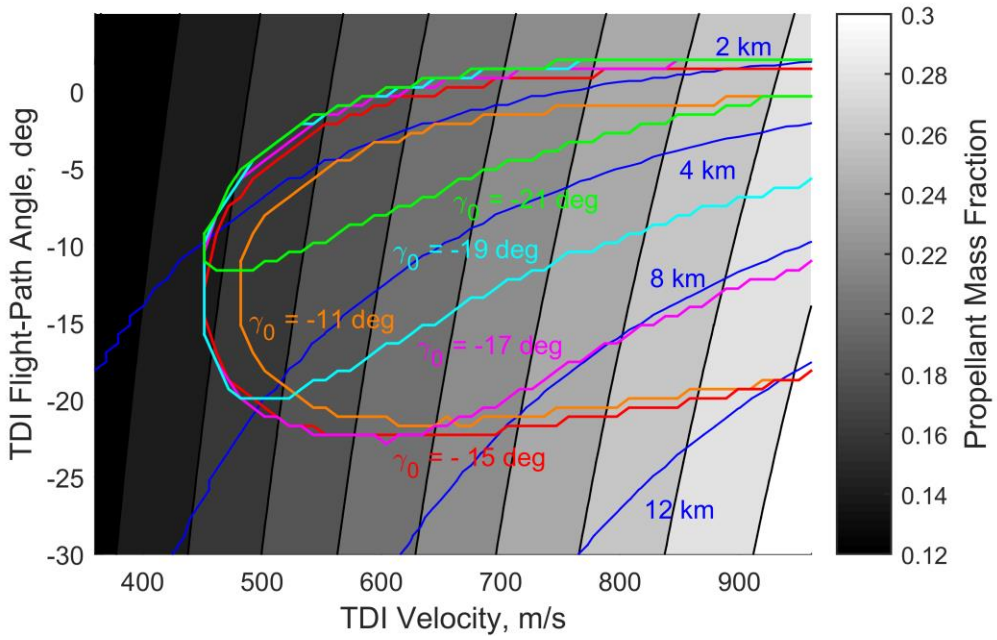

Figure 23. Reachable TDI states for several entry flight-path angles.

G. Hypersonic Control to Reachable SRP States

The reachable space provides a useful tool for identifying the feasible TDI states achievable by a hypersonic vehicle. For the region inside of the red outline in Figure 19, all of the hypersonic control histories are plotted together in Figure 24. These trajectories all successfully reached a point on the PMF-optimal supersonic retropropulsion initiation surface.

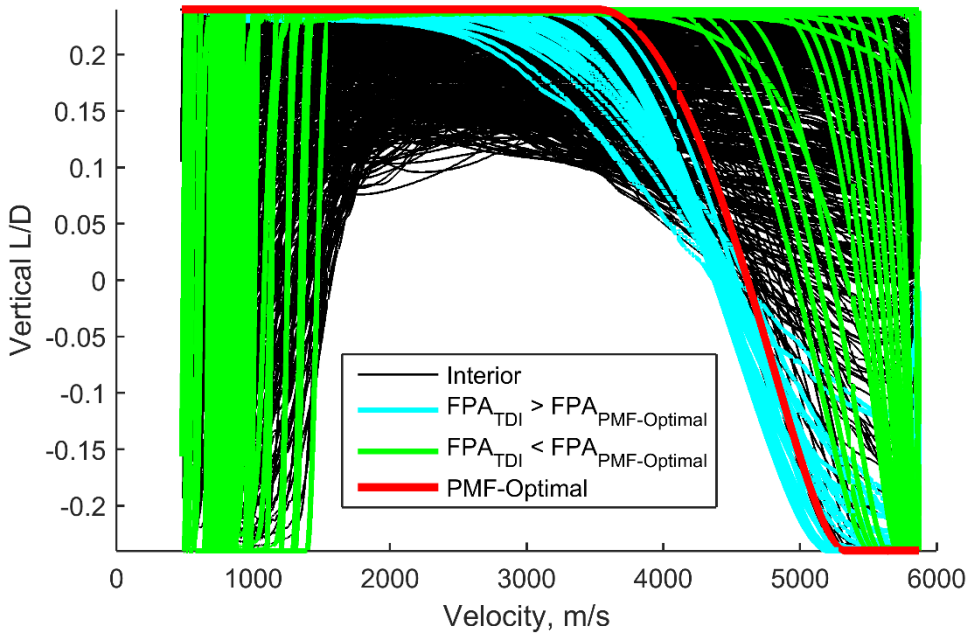

Figure 24. Trajectories within the reachable space for the nominal vehicle, location within the space indicated by color.

The trajectories on the boundary of the space are highlighted, with the shallow TDI flight-path angle trajectories at the top of the space in blue and the steep TDI flight-path angle trajectories at the bottom of the space in green. Trajectories on the bottom of the space (TDI flight-path angle between -22 and -15 deg) begin mostly lift-up, with some beginning lift-down and quickly transitioning to lift-up. These trajectories then switch to lift-down late in flight in order to achieve the targeted TDI flight-path angles. The trajectories at the top of the space (TDI flight-path angle between -15 and 2 deg), in contrast, all begin lift-down and perform a switch to lift-up as they enter deeper into the atmosphere, remaining lift-up to maintain a shallow flight-path angle at TDI. The PMF-minimizing optimal trajectory is shown in red in the figure also exhibits this single switch behavior. A bank rate constraint was added to improve convergence, giving the bank

profiles in Figure 24 a less instantaneous flip from lift-down to lift-up (and back) than the pure-bang-bang cases.

CHAPTER 4: CONCLUSIONS

Bang-bang bank-angle control can provide significant increases in terminal descent initiation altitude by beginning hypersonic flight lift-down and transitioning to lift-up at an appropriate time. A 5.5 km increase in altitude at Mach 2 was obtained for a moderate ballistic coefficient, MSL-like entry system, a significant improvement for supersonic parachute descent systems. This flight strategy was shown to be beneficial for a large range of entry vehicles over mission and vehicle design parameters of interest. Optimal control of the vehicle bank angle also enables shallower TDI flight-path angles at the expense of lower TDI altitudes.

Supersonic retropropulsion systems require different terminal descent initiation conditions than parachute descent systems. Altitude maximization at terminal descent initiation tends to create a large loft which steepens the TDI flight-path angle, increasing required propellant mass fraction for descent and landing. Optimization of supersonic retropropulsion propellant mass fraction shows that trajectories beginning lift-down and performing a single flip to lift-up minimize propellant usage during descent for many vehicle configurations and entry conditions of interest. Lower ballistic coefficients, higher lift-to-drag ratios, higher entry velocities, and steeper flight-path angles enable lower propellant mass fractions; ballistic coefficient and lift-to-drag ratio have a greater effect over the range of entry vehicles and conditions studied. Overall, these results indicate that vehicles with ballistic coefficients greater than 150 kg/m^2 may be landed at altitudes of 0 km at reasonable propellant mass fractions. A method of identifying the reachable space of TDI conditions for supersonic retropropulsion has also been outlined. The majority of trajectories that lead to feasible supersonic retropropulsion TDI points rely on either a single switch from lift-down to lift-up or two switches to reach the PMF-optimal TDI state.

REFERENCES

[1]Korzun, A. M., and Braun, R. D., "Performance Characterization of Supersonic Retropropulsion for High-Mass Mars Entry Systems," *Journal of Spacecraft and Rockets*, Vol. 47, No. 5, 2010, pp. 836-848. DOI: 10.2514/1.49803

[2]Braun, R. D., and Manning, R. M., "Mars Exploration Entry, Descent, and Landing Challenges," *Journal of Spacecraft and Rockets*, Vol. 44, No. 2, 2007, pp. 310–323. DOI: 10.2514/1.25116

[3]Braun, R. D., and Manning, R. M., "Mars Exploration Entry, Descent, and Landing Challenges," *IEEE Aerospace Conference*, IEEEAC Paper 0076, Big Sky, MT, 2006. DOI: 10.1109/AERO.2006.1655790

[4]Pritchard, E. B., and Harrison, E. F., "Lifting Entry (L/D <= 0.2) for Unmanned Viking Class Mars Landers", National Aeronautics and Space Administration, NASA TN D-5828, Washington D.C., 1970. DOI: 10.2514/6.1971-922

[5]García-Llama, E., "Apollo-Derived Terminal Control for Bank-Modulated Mars Entries with Altitude Maximization," *AIAA Guidance, Navigation and Control Conference and Exhibit*, Honolulu, HI, AIAA 2008-6819. DOI: 10.2514/6.2008-6819

[6]Lafleur, J. M., and Cerimele, C. J., "Mars Entry Bank Profile Design for Terminal State Optimization," *Journal of Spacecraft and Rockets*, Vol. 48, No. 6, 2011, pp. 1012-1024. DOI: 10.2514/1.51944

[7]Lafleur, J. M., Cerimele, C. J., "Angle of Attack Modulation for Mars Entry Terminal State Optimization," *AIAA Atmospheric Flight Mechanics Conference*, Chicago, Illinois, AIAA 2009-5611. DOI: 10.2514/6.2009-5611

[8]Benito, J., Mease, K.D., "Reachable and Controllable Sets for Planetary Entry and Landing," *Journal of Guidance, Control, and Dynamics*, Vol. 33, No. 3, 2010, pp. 641-654. DOI: 10.2514/1.47577

[9]Johnson, J. E., "Entry Heat Shield Optimization for Mars Return," *AIAA Aerospace Sciences Meeting including The New Horizons Forum and Aerospace Exposition*, Orlando, FL, AIAA 2009-518. DOI: 10.2514/6.2009-518

[10]Marinescu, A., "Isoperimetric Formulation for Some Problems of Optimization of the Entry into Atmosphere," *AIAA Journal*, Vol. 11, No. 12, 1973, pp.1768-1770. DOI: 10.2514/3.50689

[11]Marinescu, A., Manolescu, S., Pavel, M., "Minimum Heat Input Optimal Entry into Mars Atmosphere," *20th Atmospheric Flight Mechanics Conference*, Baltimore, MD, AIAA 95-3474. DOI: 10.2514/6.1995-3474

[12]Grant, M. J., Mendeck, G. F., "Mars Science Laboratory Entry Optimization Using Particle Swarm Methodology," *AIAA Atmospheric Flight Mechanics Conference and Exhibit*, Hilton Head, SC, AIAA 2007-6393. DOI: 10.2514/6.2007-6393

[13]Lu, P., "Entry Trajectory Optimization with Analytical Feedback Bank Angle Law," *AIAA Guidance, Navigation and Control Conference and Exhibit*, Honolulu, HI, AIAA 2008-7268. DOI: 10.2514/6.2008-7268

[14]Jacob, G. L., Neeler, G., Ramanan, R. V., "Mars Entry Mission Bank Profile Optimization," *Journal of Guidance, Control, and Dynamics*, Vol. 37, No. 4, 2014, pp. 1305-1316. DOI: 10.2514/1.G000089

[15]Anderson, T. R., Putnam, Z. R., and Braun, R. D., "Strategies for Landing Large Ballistic Coefficient Vehicles on Mars," *AIAA Atmospheric Flight Mechanics Conference*, San Diego, CA, AIAA 2016-0021. DOI: 10.2514/6.2016-0021

[16]Pontryagin, L. S., Boltyanskii, V. G., Gamkrelidze, R. V., and Mishchenko, E. F., *The Mathematical Theory of Optimal Processes*, Interscience, New York, 1962

[17]Patterson, M. A., and Rao, A. R., GPOPS-II – Next-Generation Optimal Control Software, Version 2.1.

[18]Cruz, J.R., et al., "Reconstruction of the Mars Science Laboratory Parachute Performance," *Journal of Spacecraft and Rockets*, Vol. 51, No.4, 2014, pp. 1185-1196. DOI: 10.2514/1.A32816

[19]Steinfeldt, B.A., "Guidance, Navigation, and Control System Performance Trades for Mars Pinpoint Landing," *Journal of Spacecraft and Rockets*, Vol. 47, No. 1, 2010, pp. 188-198. DOI: 10.2514/1.45779

[20]Edquist, K. T., Desai, P. N., Schoenenberger, M., "Aerodynamics for Mars Phoenix Entry Capsule," *Journal of Spacecraft and Rockets*, Vol. 48, No. 5, 2011, pp. 713-726. DOI: 10.2514/1.46219

[21]Justh, H. L., Justus, C. G., and Ramey, H. S., "The Next Generation of Mars-GRAM and its Role in the Autonomous Aerobraking Development Plan," *AAS/AIAA Astrodynamics Specialist Conference*, Paper 11- 478, Girdwood, AK, 2011.

[22]Korzun, A. M., Dubos, G. F., Iwata, C. K., Stahl, B. A., Quicksall, J. J., "A concept for the entry, descent and landing of high-mass payloads at Mars," *Acta Astronautica*, Vol. 66, No. 7-8, 2010, pp.1146-1159. DOI: 10.1016/j.actaastro.2009.10.003

[23]"Constellation Program Human-Systems Integration Requirements," National Aeronautics and Space Administration, CxP 70024, Revision E, Washington D.C., 2010.